High catalytic activity of $Au/CeO_x/TiO_2(110)$ controlled by the nature of the mixed-metal oxide at the nanometer level

Joon B. Park[a], Jesus Graciani[a], Jaime Evans[b], Dario Stacchiola[a], Shuguo Ma[a], Ping Liu[a], Akira Nambu[a], Javier Fernández Sanz[c], Jan Hrbek[a], and José A. Rodriguez[a,1]

[a]Chemistry Department, Brookhaven National Laboratory, Upton, NY 11973; [b]Facultad de Ciencias, Universidad Central de Venezuela, Caracas, 1020-A, Venezuela; and [c]Departamento de Química Física, Universidad de Sevilla, E-41012-Seville, Spain

Edited by Gabor A. Somorjai, University of California, Berkeley, CA, and approved January 30, 2009 (received for review December 11, 2008)

Mixed-metal oxides play a very important role in many areas of chemistry, physics, materials science, and geochemistry. Recently, there has been a strong interest in understanding phenomena associated with the deposition of oxide nanoparticles on the surface of a second (host) oxide. Here, scanning tunneling microscopy, photoemission, and density-functional calculations are used to study the behavior of ceria nanoparticles deposited on a $TiO_2(110)$ surface. The titania substrate imposes nontypical coordination modes on the ceria nanoparticles. In the $CeO_x/TiO_2(110)$ systems, the Ce cations adopt an structural geometry and an oxidation state (+3) that are quite different from those seen in bulk ceria or for ceria nanoparticles deposited on metal substrates. The increase in the stability of the Ce^{3+} oxidation state leads to an enhancement in the chemical and catalytic activity of the ceria nanoparticles. The codeposition of ceria and gold nanoparticles on a $TiO_2(110)$ substrate generates catalysts with an extremely high activity for the production of hydrogen through the water–gas shift reaction ($H_2O + CO \rightarrow H_2 + CO_2$) or for the oxidation of carbon monoxide ($2CO + O_2 \rightarrow 2CO_2$). The enhanced stability of the Ce^{3+} state is an example of structural promotion in catalysis described here on the atomic level. The exploration of mixed-metal oxides at the nanometer level may open avenues for optimizing catalysts through stabilization of unconventional surface structures with special chemical activity.

heterogeneous catalysis | imaging | structural properties | surface reactivity

Mixed-metal oxides play a very important role in many areas of chemistry, physics, materials science, and geochemistry (1–6). In technological applications, they are used in the fabrication of microelectronic circuits, piezoelectric devices, and sensors and as catalysts. Over the years, there has been a strong interest in understanding the behavior of mixed-metal oxides at a fundamental level (1–3). What happens when nanoparticles (NPs) of a given metal oxide are deposited on the surface of a second (host) oxide (3, 7)? In principle, the combination of 2 metals in an oxide matrix can produce materials with novel structural and/or electronic properties. At a structural level, a dopant can introduce stress into the lattice of an oxide host, inducing in this way the formation of defects. On the other hand, the lattice of the oxide host can impose on the dopant element nontypical coordination modes. Finally, metal ↔ metal or metal ↔ oxygen ↔ metal interactions in mixed-metal oxides can give electronic states not seen in single-metal oxides.

In this article, we use photoemission, scanning tunneling microscopy (STM), and calculations based on density-functional theory (DFT) to study the behavior of ceria NPs in contact with $TiO_2(110)$. Ceria and titania are among the most widely used oxides in catalysis (1, 4–6, 8–12). These oxides are important components in catalysts used for the production of clean hydrogen through the water–gas shift reaction ($H_2O + CO \rightarrow H_2 + CO_2$) and for the oxidation of carbon monoxide ($2CO + O_2 \rightarrow 2CO_2$). Ceria and titania adopt different crystal lattices in their most stable bulk phases, fluorite and rutile, respectively (2, 13). Within the fluorite structure each Ce atom is bonded to 8 O atoms, whereas 6 O atoms surround the Ti atoms in the rutile structure. One of the most interesting properties of ceria is its ability to undergo a conversion between "+4" and "+3" formal oxidation states (13). The surface chemistry and catalytic properties of CeO_2 depend on the formation of Ce^{3+} ions (13), and different approaches are followed to maximize their concentration (4, 5, 8). In the $CeO_x/TiO_2(110)$ systems, the titania substrate imposes on the ceria NPs nontypical coordination modes with a subsequent change in the relative stability of the Ce^{3+}/Ce^{4+} oxidation states that leads to a significant enhancement in chemical activity. Furthermore, the deposition of gold NPs on $CeO_x/TiO_2(110)$ produces surfaces with an extremely high catalytic activity for the water–gas shift reaction and the oxidation of CO. This is quite remarkable because neither $Au/TiO_2(110)$ nor $Au/CeO_2(111)$ come close to matching the catalytic activity of $Au/CeO_x/TiO_2(110)$.

Experimental and Theoretical Methods

Microscopy, Photoemission, and Catalytic Tests. The microscopy studies were carried out in an Omicron variable temperature STM system that is directly attached to a main ultrahigh vacuum (UHV) chamber equipped with optics for low-energy electron diffraction, instrumentation for Auger electron spectroscopy and surface cleaning facilities (9, 14). Chemically etched W tips were used for imaging the surfaces. The $TiO_2(110)$ crystal was cleaned by several cycles of Ne^+ sputtering (1 keV, 40 min) and annealing (950 K, 5 min), and XPS/AES studies confirmed that there were no surface contaminants after this treatment (15).

Furthermore, the high-resolution STM images of the surface exhibited bright Ti rows separated by 6.5 Å, as typically observed for $TiO_2(110)$-(1x1) (16). Photoemission studies were performed at beamline U7A of the National Synchrotron Light Source (NSLS) at Brookhaven National Laboratory (9) by using a photon energy of 625 eV to collect the O 1s and Ti 2p regions, and 325 eV to collect the Ce 4d, Au 4f, and valence regions. In a separate UHV chamber, we acquired XPS spectra (Ce 3d, Ti 2p, O 1s, and Au 4f regions) and UPS spectra (valence region) using Mg Kα and He-I radiation, respectively. Ce and Au were deposited on $TiO_2(110)$ by using metal evaporators (9, 14, 17). The flux of the Au doser was calibrated by depositing Au onto a Mo(100) crystal and measuring the thermal desorption spectra of the admetal (17). The area of the titania surface covered by ceria

Author contributions: J.B.P., J.G., J.E., D.S., S.M., P.L., A.N., J.F.S., J.H., and J.A.R. designed research; J.B.P., J.G., J.E., D.S., S.M., A.N., and J.A.R. performed research; J.B.P., J.G., J.E., D.S., S.M., P.L., A.N., J.F.S., J.H., and J.A.R. analyzed data; and J.A.R. wrote the paper.

The authors declare no conflict of interest.

This article is a PNAS Direct Submission.

[1]To whom correspondence should be addressed. E-mail: rodrigez@bnl.gov.

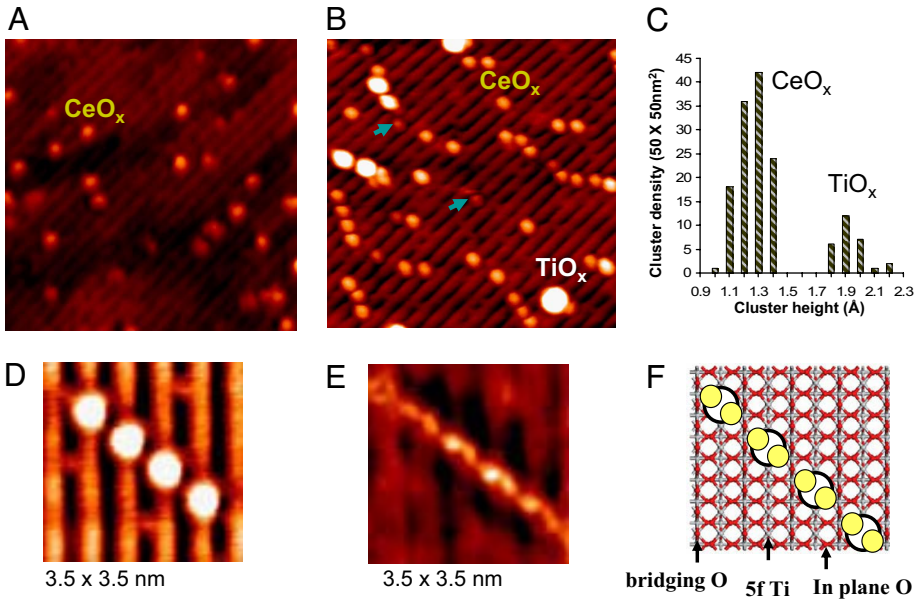

Fig. 1. STM results illustrating morphological changes of CeO_x on the TiO_2(110) surface. (*A*) STM image (15 × 15 nm) taken after depositing Ce atoms at 298 K in UHV (V_t = 1.3 V and I_t = 0.05 nA). (*B*) STM image (15 × 15 nm) acquired after depositing Ce atoms at 600 K and subsequent annealing at 900 K in O_2 (P_{O2} ≈1 × 10^{-7} Torr) (V_t = 1.2 V and I_t = 0.07 nA). (*C*) Height distribution for the spots seen in *B*. (*D* and *E*) Zoomed-in STM images (3.5 × 3.5 nm) of a diagonal array of CeO_x taken at different imaging condition of 1.2 V, 0.06 nA and 0.4 V, 0.06 nA, respectively. (*F*) Model showing possible orientations for the bright protrusions of CeO_x in *D* and *E*. The dimers of ceria are shown as a combination of white and yellow spheres.

and gold was estimated by using STM images or a combination of ion-scattering spectroscopy (ISS) and photoemission (9, 17).

The catalytic studies were carried out in a system that combines a batch reactor and a UHV chamber (9, 17). The sample could be transferred between the reactor and UHV chamber without exposure to air. Typically, it was transferred to the batch reactor at ≈298 K, and then the reactant gases were introduced (water–gas shift: 20 Torr of CO and 10 Torr of H_2O; CO oxidation: 4 torr of CO and 2 Torr of O_2). The catalytic activity for the water–gas shift was measured at 625 K (9, 17), with a temperature of 300 K for the oxidation of CO (10). Product yields were analyzed by gas chromatography or mass spectroscopy (9, 17). The amount of molecules produced was normalized by the active area exposed by the sample. In our reactor, a steady-state regime for the water–gas shift or the oxidation of CO was reached after 2–3 min of reaction time.

DFT Calculations. Periodic DFT + U calculations were performed by using the VASP code (18) using a (4 × 2) 6-layer thick supercell to model the TiO_2(110) surface (19). The adlayer and first 4 layers of the titania slab were allowed to relax during the DFT geometry optimizations. We used the Perdew–Wang 91 GGA functional for exchange-correlation, the projector-augmented wave approach, and plane-waves with a cutoff energy set at 400 eV. We treated the Ti (3s, 3p, 3d, 4s), Ce (4f, 5s, 5p, 5d, 6s), and O (2s,2p) electrons as valence states, whereas the remaining electrons were kept frozen as core states (19). The calculations were performed at the Γ point of the Brillouin zone (18). To reproduce the valence spectra of Ce/TiO_2(110), see below, we used U_{eff} parameters with a value of 4.5 eV for Ce and Ti. This value is close to those used in previous studies for bulk ceria or titania (20). The introduction of the U_{eff} parameters in the DFT calculations was found to be essential to correctly reproduce the position of the occupied Ce 4f and Ti 3d levels in the valence region, even though the trends found in the energetics for the coadsorption of Ce and O on TiO_2(110) were almost the same with or without the U_{eff} parameters.

Growth of Ceria on TiO_2(110)

In Fig. 1, we show STM images acquired after depositing cerium on TiO_2(110) under different conditions. Fig. 1*A* corresponds to an image obtained after dosing Ce atoms under ultrahigh vacuum (UHV) at a sample temperature of 298 K. The bright spots have an average height of 1.4 ± 0.2 Å over the flat terrace and correspond to clusters of cerium oxide. The corresponding XPS and UPS spectra indicated that cerium was in an oxidation state of +3, and, consequently, its deposition led to the partial reduction of titanium cations with the appearance of Ti^{3+}. Fig. 2 *Left* shows a typical UPS spectrum for this type of Ce/TiO_2(110) surface. The features ≈1 eV can be assigned to Ti^{3+} centers (1, 16), whereas those at 2–3.5 eV correspond to Ce^{3+} centers (21). The existence of Ce^{3+} is corroborated by the Ce 3d XPS data in Fig. 2 *Right*. The Ce 3d XPS spectrum for the as-prepared Ce/TiO_2(110) surface has the distinctive line shape of Ce^{3+} species (21, 22). Using DFT calculations, we investigated the bonding of Ce atoms to the TiO_2(110) surface. The Ce atoms prefer the bonding configuration shown at the bottom of Fig. 2, interacting simultaneously with bridging and in-plane O atoms of the titania substrate. Upon adsorption, Ce formally releases 3 electrons to the oxide host, which move from the 6s and 5d levels in Ce to the lower-energy 3d levels in Ti, reducing 3 Ti^{4+} cations to Ti^{3+}. The fourth valence electron from Ce is in a 4f level of lower energy than the 3d from Ti and therefore is not transferred, leaving the oxidation state of Ce as 3+. The adsorption of oxygen on the Ce/TiO_2(110) surfaces led to the disappearance of Ti^{3+} sites in the XPS/UPS spectra and in the DFT-calculated density of states. The stability of the Ce^{3+} cations was verified by their resistance to oxidation under UHV conditions. We had to expose the Ce/TiO_2(110) surfaces to an O_2 pressure of 1 Torr in the batch reactor to obtain the typical Ce 3d XPS spectrum of Ce^{4+} cations (21, 22), see Fig. 2 *Right*.

To avoid the reduction of the titania substrate, Ce atoms were deposited at 600 K and annealed to 900 K under O_2 (≈1 × 10^{-7} Torr) for 5 min. This led to the image shown in Fig. 1*B*. In this image, the features nonrelated to the ideal TiO_2(110) surface can be separated according to their height, as seen in Fig. 1*C*. Most of the spots (≈80%) have a height of 1.3 ± 0.2 Å. These spots

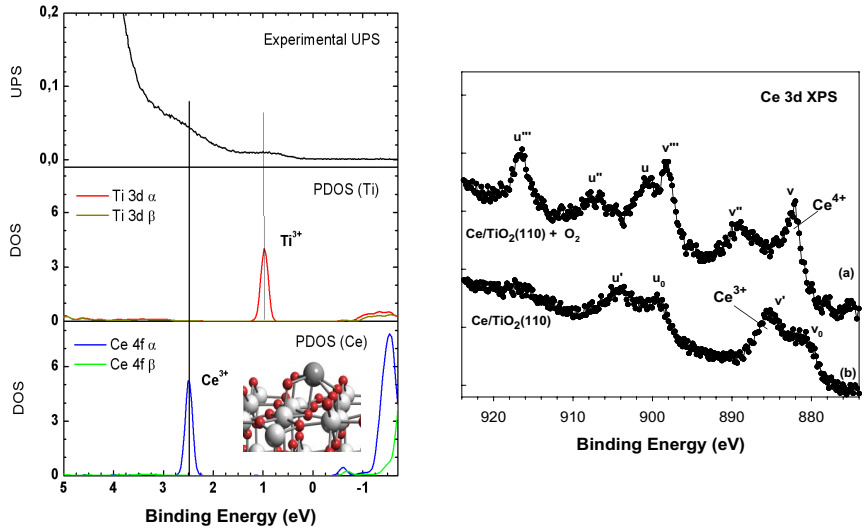

Fig. 2. Electronic properties of CeO_x/TiO_2 (110). (*Left*) (*Top*) Shown is a UPS spectrum acquired after depositing Ce atoms on TiO_2(110) at 298 K. The features marked by vertical lines are not seen on clean stoichiometric TiO_2(110). (*Middle* and *Bottom*) Displayed are DFT calculated density-of-states (DOS) for a Ce/TiO_2(110) surface, including occupied (positive binding energy) and unoccupied states (negative binding energy, states not observable in UPS). The drawing in the *Inset* shows the bonding configuration of the Ce atoms. Color code for spheres is gray, cerium; red, oxygen; white, titanium. (*Right*) Ce 3d XPS spectra taken after depositing Ce on TiO_2(110) at 298 K (lower), with subsequent exposure to 1 Torr of O_2 (upper). The change in the line shape denotes a $Ce^{3+} \rightarrow Ce^{4+}$ transformation (21, 22). The ''u'' and ''v'' peaks refer to various final states that are caused by transitions from valence band electrons into Ce 4f states (22).

can be attributed to CeO_x, after comparing with the image in Fig. 1*A* for Ce/TiO_2(110). A minority of the spots (≈20%) in Fig. 1*B* have a height of 1.9 ± 0.3 Å. These features were not seen for Ce/TiO_2(110) and probably correspond to (1 × 2) reconstructions of TiO_2(110) induced by O_2 chemisorption (11, 16). They are a consequence of the migration of interstitial Ti atoms from the bulk to the surface of the titania crystal (11, 16). We found them also in blank experiments for O_2/TiO_2(110). In Fig. 1*B*, the spots due to CeO_x are arranged forming units that are oriented ≈48°, 66°, or 90° with respect to the Ti rows of the oxide substrate. These units were not seen in blank experiments for Ce/TiO_2(110) or O_2/TiO_2(110) and are characteristic of the $O_2/CeO_x/TiO_2$(110) systems. Close-up images of a ≈44° aligned unit are shown in Fig. 1 *D* and *E*. In Fig. 1*D*, the bright ceria spots are centered on 5f Ti rows and all have a height close to 1.35 Å and a diameter of 6.8 Å. Their size and position suggests that each spot may contain 2 Ce atoms located in between the O bridging and 5f Ti rows. This is confirmed by scanning the same feature with lower imaging bias (0.4 V instead of 1.2 V), where the electron tunneling occurs at different density of states in CeO_x/TiO_2(110) systems (Fig. 1*E*). From the STM data, one can construct a structural model consisting of an array of dimers of ceria as displayed in Fig. 1*F*. According to our measurements of core and valence photoemission, the oxidation state of the Ce atoms inside the dimers is essentially +3. Thus, in the CeO_x/TiO_2(110) systems, the Ce cations adopt a structural geometry and an oxidation state that are quite different from those seen in bulk ceria (2, 13) or for NPs of ceria deposited on metal substrates (7, 9).

Using DFT, we investigated the process of adsorption–oxidation for Ce deposited on TiO_2(110). Fig. 3 shows the calculated energy pathway for such a process. The adsorption energy of atomic Ce is very high ($\Delta E = -7.23$ eV). On its most stable adsorption site, Ce interacts with 2 bridging and 1 in-plane O atoms (Fig. 3, step1). The fact that 3 electrons move from high to lower energy levels, $Ce(5d^16s^2) \rightarrow Ti(3d^1)$, explains in part the high adsorption energy of Ce. The adsorption process of atomic Ce could be described as

$$Ce + 3Ti^{4+}(TiO_2) \rightarrow Ce^{3+} + 3Ti^{3+}(TiO_2) \qquad [1]$$

The dissociation of O_2 near the adsorbed Ce is a highly exothermic process ($\Delta E = -6.66$ eV). The final structure is a unit of CeO_2 over TiO_2(110), where the O atoms are adsorbed on top of in-plane Ti atoms and strongly interact with the Ce atom (Fig. 3, step 2). The oxidation state of the Ce in this configuration is 4+

$$Ce^{3+} + 3Ti^{3+}(TiO_2) + O_2 \rightarrow CeO_2(Ce^{4+})/TiO_2 \qquad [2]$$

Such CeO_2 monomers could be assigned to the smallest spots observed in STM at very low coverages of ceria. For the surface in Fig. 1*B*, possible CeO_2 monomers are denoted by arrows and, as predicted by the DFT calculations, they are not located at the center of the Ti rows. The CeO_2 monomers are excellent sites for

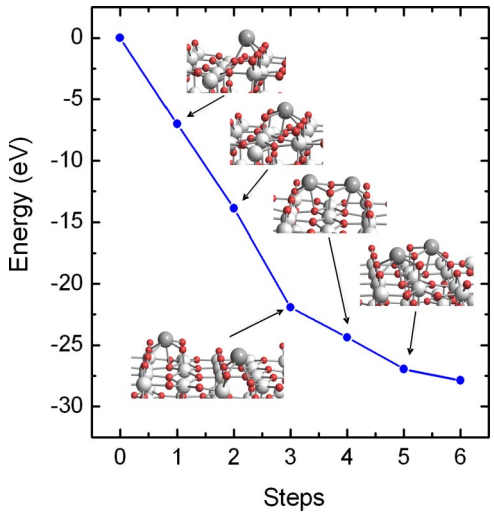

Fig. 3. DFT calculated energy pathway for the adsorption and oxidation of Ce on TiO_2(110). The following steps were examined: (1) adsorption of Ce; (2) O_2 adsorption-dissociation and formation of the first monomer (CeO_2); (3) adsorption of a second cerium atom; (4) formation of the first Ce_2O_2 dimer; (5) adsorption of ½O_2 and formation of the Ce_2O_3 dimer; and (6) adsorption of ½O_2 and formation of 2 CeO_2 monomers.

the adsorption of a second Ce atom to form dimers (Fig. 3, step 4). The increment in the adsorption energy with respect to the adsorption on a clean surface is due to the fact that 1 of the 3 electrons released by the incoming Ce does not go to the high-energy 3d levels of Ti but rather to the 4f of Ce^{4+} from the CeO_2 monomer, which is reduced to Ce^{3+}

$$CeO_2(Ce^{4+})/TiO_2 + Ce + 2Ti^{4+}(TiO_2) \rightarrow Ce_2O_2(Ce^{3+}) \text{ on } TiO_2 + 2Ti^{3+}(TiO_2) \quad [3]$$

The addition of oxygen to the Ce_2O_2 unit generates Ce_2O_3.

$$Ce_2O_2(Ce^{3+})/TiO_2 + 2Ti^{3+}(TiO_2) + \frac{1}{2}O_2 \rightarrow Ce_2O_3(Ce^{3+}) \quad [4]$$

on TiO_2, and the ceria dimer adopts a configuration (Fig. 3, step 5) where shared oxygen leads to a diagonal arrangement in agreement with the results of STM (Fig. 1 *E* and *F*). In the presence of oxygen, the complete oxidation of Ce has to be considered, going from a Ce_2O_3 dimer to 2 CeO_2 monomers (Fig. 3, step 6). Differently from the previous step, here, there are not high-energy Ti 3d electrons but 2 electrons in low-energy Ce 4f states. The process is exothermic but only by −0.92 eV, 3 times less than the energy released in the previous step. This means that as long as Ti^{3+} species exist, O_2 will prefer to adsorb and dissociate on them because the stabilization energy for the system is much higher. Therefore, even though the oxidation process of dimers is favorable, the other site is preferred for the adsorption and dissociation of O_2. This illustrates the complex interplay that one can have when dealing with the electronic and chemical properties of a mixed-metal oxide.

For applications in catalysis, the relative stability of the Ce^{3+}/Ce^{4+} oxidation states of ceria is a very important issue (1, 4–6, 13, 23, 24). We calculated the energy released by the reactions

$$Ce_2O_3 + \frac{1}{2}O_2 \rightarrow 2CeO_2 \quad [5]$$

$$2CeO_2 + CO \rightarrow Ce_2O_3 + CO_2 \quad [6]$$

for both bulk ceria and Ce_2O_3 dimers deposited on TiO_2(110). The ΔE for the oxidation process, (the reaction shown in **5**), was −2.56 eV in the case of bulk Ce_2O_3 and −0.92 eV for the Ce_2O_3 dimers bonded to titania. The reduction of CeO_2/TiO_2(110) by CO, (the reaction shown in **6**), was a very exothermic process with a ΔE of −2.35 eV. In contrast, the ΔE for the corresponding reaction of bulk CeO_2 was −0.71 eV. These trends were confirmed by comparing reduction/oxidation experiments on CeO_2 (111) and CeO_x/TiO_2(110). For example, a CeO_2(111) surface did not undergo reduction under an atmosphere of 20 Torr of CO at 400 K (17), but a CeO_2/TiO_2(110) surface (formed by exposing CeO_x/TiO_2(110) to 1 Torr of O_2 at 298 K) was completely transformed into Ce_2O_3/TiO_2(110). The high stability of the Ce^{3+} cations in CeO_x/TiO_2(110) is a consequence of their nontypical coordination mode and the effect of Ce (4f)–O (2p)–Ti (3d) bonding interactions.

Catalytic Activity of $Au/CeO_x/TiO_2$(110)

The WGS reaction is a critical catalytic process for the production of clean hydrogen in the chemical industry (4, 5). There is a continuous search for catalysts with a better WGS activity (4–6, 9). As shown below, the deposition of gold NPs on CeO_x/TiO_2(110) yielded surfaces with an extremely high catalytic activity for the WGS. Fig. 4 displays STM images acquired from the same surface area before (Fig. 4*A*) and after (Fig. 4*B*) depositing gold on CeO_x/TiO_2(110) at 298 K with subsequent annealing to 600 K (Fig. 4*C*). The CeO_x/TiO_2(110) was preannealed under O_2 (≈1 × 10^{-7} Torr) at 900 K and had a morphology similar to that seen in Fig. 1*B*. The deposition of Au at room temperature, ≈0.2 monolayer, produced 3-dimensional metal particles anchored to steps of the titania surface, "a" sites, to the (1 × 2) reconstructions of TiO_2(110), "b" sites, and to the CeO_x dimers, "c" sites. Annealing to 600 K produced large particles of Au that were simultaneously located on b and c sites. Au NPs with a diameter as large as 5.9 nm and a height of 1.3 nm were seen, but smaller metal particles were also present on the CeO_x/TiO_2(110) surface. On this surface, the dispersion of the Au NPs was substantially larger than seen on a pure TiO_2(110) surface where Au mainly binds to the steps (10, 15).

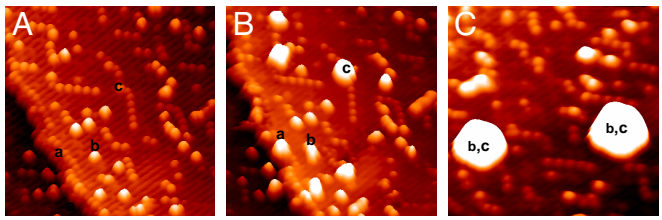

Fig. 4. Morphology of $Au/CeO_x/TiO_2$ (110). (*A*) STM image of a CeO_x/TiO_2(110) surface. Ce was deposited at 600 K under an atmosphere of O_2 (≈1 × 10^{-7} Torr) and then the sample was annealed at 900 K in O_2. (*B*) STM image for a $Au/CeO_x/TiO_2$(110) surface. The gold was deposited on the same area shown in *A* at 298 K. Approximately 6% of the surface was covered with Au. (*C*) STM image obtained after annealing the system in *B* to 600 K. All of the STM images correspond to an area of 20 × 20 nm and imaging conditions of V_t = 1.5 V and I_t = 0.03 nA.

Neither CeO_x/TiO_2(110) nor Au(111) were able to catalyze the WGS. However, $Au/CeO_x/TiO_2$(110) surfaces are outstanding catalysts for the WGS as shown in Fig. 5. We performed test experiments in which Au/TiO_2(110) surfaces were prepared following the same steps used for the synthesis of $Au/CeO_x/TiO_2$(110) but without the deposition of cerium. The Au/TiO_2(110) systems were good WGS catalysts, see Fig. 5 *Upper*, but they did not come close to match the activity of $Au/CeO_x/TiO_2$(110). The same is valid when comparing with the WGS activities of Au/CeO_2(111) (17), CeO_x/Au(111) (9), Cu/ZnO(0001) (17), and copper single crystals (17, 25). Cu/ZnO is the most common WGS catalyst used in the industry (5, 17, 25), and copper is the best pure-metal catalyst (25, 26). For the $Au/CeO_x/TiO_2$(110) catalyst in Fig. 5, one could assume that the concentration of active sites is proportional to the number of ceria regions in contact with gold NPs. Because only 12% of the titania support was covered by ceria, as measured by ion scattering spectroscopy (ISS), the $Au/CeO_x/TiO_2$(110) catalyst must be at least 300 times more active than a Cu (100) surface on a per-active-site basis.*

Postreaction characterization of the $Au/CeO_x/TiO_2$(110) surfaces with XPS showed the presence of metallic Au and Ce^{3+} cations. An identical result was found in in situ measurements of X-ray absorption spectroscopy for $Au/CeO_x/TiO_2$ powders under

*It is usually assumed that all atoms of a flat Cu(100) surface, 1.53 × 10^{15} atoms cm^{-2}, are active in the WGS reaction (25). The structural model in Fig. 1*F* was used to calculate the area occupied by a Ce_2O_3 dimer on the TiO_2(110) surface. Using this and the ceria coverage determined from ISS measurements (≈12% of the titania surface was covered), we find that the concentration of Ce in the $Au/CeO_x/TiO_2$(110) catalyst of Fig. 5 was in the order of 0.03 × 10^{15} atoms cm^{-2}. This is an upper limit to the actual concentration of the active sites, because not all of the Ce atoms had a Au particle nearby (see Fig. 4 *B* and *C*). After subtracting the WGS activity of Au/TiO_2(110) from that of $Au/CeO_x/TiO_2$(110), one finds that the Au/ceria sites are at least 300 times more active than the atoms in a Cu(100) surface.

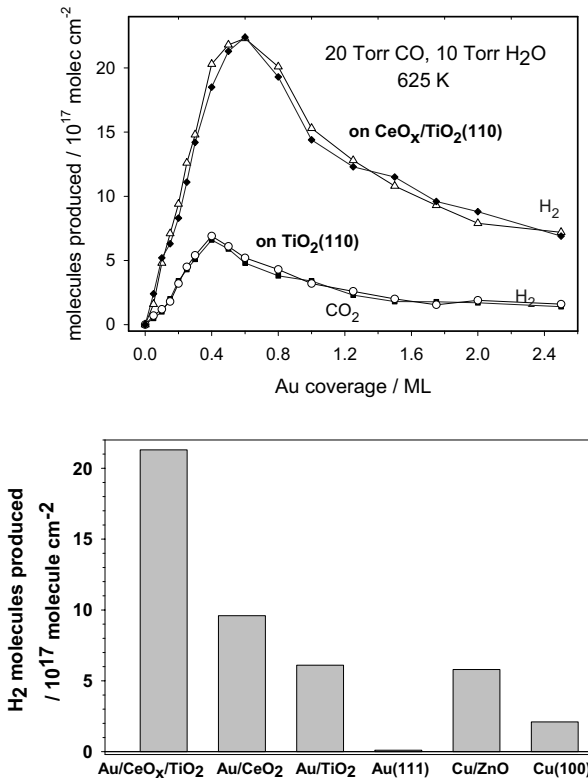

Fig. 5. Water-gas shift catalysis. (*Upper*) Water–gas shift activity of Au/TiO_2(110) and Au/CeO_x/TiO_2(110) as a function of Au coverage. The area of TiO_2(110) covered by CeO_x was measured with ISS, before depositing gold, and found to be ≈12% of the clean substrate. The reported values for the production of H_2 (blue curve) and CO_2 (black curve) were obtained after exposing the catalysts to 20 Torr of CO and 10 Torr of H_2O at 625 K for 5 min. The number of H_2 and CO_2 molecules produced is normalized by the sample surface area. (*Lower*) Comparison of the water–gas shift activity of Cu(100), Au(111), and 0.5 mL of Au supported on TiO_2(110), CeO_2(111) or CeO_x/TiO_2(110). The data for Cu(100), Cu/ZnO(0001) and Au/CeO_2(111) were taken from ref. 17.

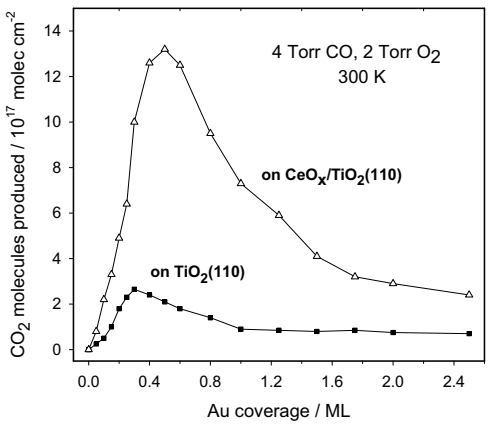

Fig. 6. CO oxidation activity of Au/TiO_2(110) and Au/CeO_x/TiO_2(110) as a function of Au coverage. The area of TiO_2(110) covered by CeO_x was measured with ISS, before depositing gold, and found to be ≈16% of the clean substrate. The reported values for the production of CO_2 were obtained after exposing the catalysts to 4 Torr of CO and 2 Torr of O_2 at 300 K for 5 min. The number of CO_2 molecules produced is normalized by the sample surface area.

WGS reaction conditions. The high catalytic activity of Au/CeO_x/TiO_2(110) can be attributed to the special chemical properties of the supported Ce_2O_3 dimers and cooperative effects at ceria–gold interfaces. Usually, the rate-determining step in the WGS reaction is the dissociation of water (9, 17, 26). Isolated NPs of gold cannot dissociate this molecule (27, 28). We found that the Ce^{3+} sites present in CeO_x/TiO_2(110) easily dissociate water, but, upon exposure to CO, highly stable HCO_x species were formed on the oxide surface and there was no production of H_2 or CO_2 gas. In Au/CeO_x/TiO_2(110), one has a bifunctional catalyst: The adsorption and dissociation of water takes place on the oxide, CO adsorbs on gold NP sites, and all subsequent reaction steps occur at oxide–metal interfaces. Au NPs do catalyze the reaction of OH with CO to yield a HOCO intermediate and then H_2 and CO_2 (27). Previous studies for the WGS on Au–CeO_2 catalysts point to a direct participation of the oxide in the reaction process (4, 5, 9). Our results illustrate the tremendous impact that an optimization of the chemical properties of nanoceria can have on the activity of a WGS catalyst.

Nowadays, the oxidation of CO on Au/TiO_2 catalysts is receiving a lot of attention (1, 10, 29, 30). Fig. 6 displays the CO oxidation activity of Au/TiO_2(110) and Au/CeO_x/TiO_2(110) as a function of Au coverage. In the case of Au/TiO_2(110) a maximum in the production of CO_2 is seen at a Au coverage of ≈0.3 mL. Previous studies have shown that there is a marked size effect on the catalytic activity, with Au clusters in the range of 3–3.5 nm exhibiting the maximum reactivity (10, 29). Our STM studies for Au/TiO_2(110) and Au/CeO_x/TiO_2(110) also show a strong variation in catalytic activity with Au particle size. In all cases, Au/CeO_x/TiO_2(110) is a much better catalyst for the oxidation of CO than Au/TiO_2(110). If the maximum catalytic activities seen in Fig. 6 are normalized by the number of Au atoms present on the oxide supports (10, 29), we estimate turnover frequencies (TOFs) for CO oxidation of 2.1 molecules per site^{-1} s^{-1} for Au/TiO_2(110) and 6.2 molecules per site^{-1} s^{-1} for Au/CeO_x/TiO_2(110). These should be taken as lower limits for the TOFs because we probably overestimated the number of exposed Au active sites. Here, we are following previous studies (10, 29) that estimate the TOFs assuming total dispersion of Au on the oxide substrate. In any case, the TOF of Au/CeO_x/TiO_2(110) is already larger than the TOF found, under similar conditions of pressure and temperature, for the oxidation of CO on a highly active Au ultrathin film supported on a reduced TiO_x substrate: ≈4 molecules per site^{-1} s^{-1} (30).

The rate-limiting step for the oxidation of CO on Au/oxide surfaces is the activation and dissociation of the O_2 molecule (31–33). The oxide probably helps in the stabilization of an OC·O_2 intermediate and the breaking of the O–O bond. The structure of the titania supported ceria nanoparticles should facilitate their direct interaction with an OC·O_2 intermediate. Postreaction surface analysis with XPS showed the presence of a significant amount of Ce^{3+} in the Au/CeO_x/TiO_2(110) catalysts. This and a relatively high dispersion of Au (Fig. 4*B*) could be responsible for the superior activity of Au/CeO_x/TiO_2(110) during the oxidation of CO at room temperature.

Summary and Conclusions

Scanning tunneling microscopy, photoemission, and density-functional calculations were used to study the behavior of ceria nanoparticles deposited on a TiO_2(110) surface. The titania substrate imposes nontypical coordination modes on the ceria nanoparticles. In the CeO_x/TiO_2(110) systems, the Ce cations adopt an structural geometry and an oxidation state (+3) that are quite different from those seen in bulk ceria or for ceria nanoparticles deposited on metal substrates. The increase in the stability of the Ce^{3+} oxidation state leads to an enhancement in the chemical and catalytic activity of the ceria nanoparticles. The codeposition of ceria and gold nanoparticles on a TiO_2(110) substrate generates catalysts with an extremely high activity for the production of hydrogen through the water–gas shift reaction ($H_2O + CO \rightarrow H_2 + CO_2$) or for the oxidation of carbon monoxide ($2CO + O_2 \rightarrow$

$2CO_2$). Our results illustrate the high impact that an optimization of the chemical properties of nanoceria can have on the activity of a WGS or CO oxidation catalyst. This approach should be valid in general for catalysts that contain ceria as part of a mixed-metal oxide (4–7), opening new directions for tuning catalytic activity by coupling appropriate pairs of oxides. The key issue is to take advantage of the complex interactions that occur in a mixed-metal oxide at the nanometer level.

ACKNOWLEDGMENTS. We thank M. Pérez for thought-provoking discussions about the mechanism for the WGS reaction on $Au/CeO_x/TiO_2(110)$. The work performed at Brookhaven National Laboratory was supported by the U.S. Department of Energy, Office of Basic Energy Sciences under contract DE-AC02-98CH10886. J.E. is grateful to the Instituto de Tecnología Venezolana para el Petróleo for partial support of the work carried out at the Universidad Central de Venezuela. The work done at Seville was funded by Ministry of Science and Innovation Grant MAT2008-04918 and Barcelona Supercomputing Center—Centro Nacional de Supercomputación (Spain).

1. Zhou B, Hermans S, Somorjai GA, eds (2004) *Nanotechnology in Catalysis* (Kluwer–Plenum, New York).
2. Rao CNR, Raveau B (1998) *Transition Metal Oxides: Structure, Properties and Synthesis of Ceramic Oxides* (Wiley, New York), 2nd Ed.
3. Knauth P, Schoonman J, eds (2002) *Nanocrystalline Metals and Oxides: Selected Properties and Applications* (Springer, Berlin).
4. Fu Q, Saltsburg H, Flytzani-Stephanopoulos M (2003) Active nonmetallic Au and Pt species on ceria-based water–gas shift catalysts. *Science* 301:935–938.
5. Burch R (2006) Gold catalysts for pure hydrogen production in the water–gas shift reaction: Activity, structure and reaction mechanism. *Phys Chem Chem Phys* 8:5483–5500.
6. Gonzalez ID, Navarro RM, Alvarez-Galvan MC, Rosa F, Fierro JLG (2008) Performance enhancement in the water–gas shift reaction of platinum deposited over a cerium-modified TiO_2 support. *Catal Commun* 9:1759–1765.
7. Fernández-García M, Martinez-Arias A, Hanson JC, Rodriguez JA (2004) Nanostructured oxides in chemistry: Characterization and properties. *Chem Rev* 104:4063–4104.
8. Esch F, et al. (2005) Electron localization determines defect formation on ceria substrates. *Science* 309:752–755.
9. Rodriguez JA, et al. (2007) Activity of CeO_x and TiO_x nanoparticles grown on Au(111) in the water–gas shift reaction. *Science* 318:1757–1760.
10. Valden M, Lai X, Goodman DW (1998) Onset of catalytic activity of gold clusters on titania with the appearance of nonmetallic properties. *Science* 281:1647–1650.
11. Wendt S, et al. (2008) The role of interstitial sites in the Ti3d defect state in the band gap of titania. *Science* 320:1755–1759.
12. Diwald O, Thompson TL, Goralski EG, Walck SD, Yates JT (2004) The effect of nitrogen ion implantation on the photoactivity of TiO_2 rutile single crystals. *J Phys Chem B* 108:52–57.
13. Trovarelli A (1996) Catalytic properties of ceria and CeO_2-containing materials. *Catal Rev Sci Eng* 38:439–520.
14. Ma S, Rodriguez JA, Hrbek J (2008) STM study of the growth of cerium oxide nanoparticles on Au(111). *Surf Sci* 602:3272–3279.
15. Park JB, Conner SF, Chen DA (2008) Bimetallic Pt-Au clusters on $TiO_2(110)$: Growth, surface composition, and metal-support interactions. *J Phys Chem C* 112:5490–5500.
16. Diebold U (2003) The surface science of titanium dioxide. *Surf Sci Rep* 48:53–229.
17. Rodriguez JA, et al. (2007) Water gas shift reaction on Cu and Au nanoparticles supported on $CeO_2(111)$ and $ZnO(000\bar{1})$: Intrinsic activity and importance of support interactions. *Angew Chem Int Ed* 46:1329–1332.
18. Kresse G, Furthmuller J (1996) Efficiency of ab-initio total energy calculations for metals and semiconductors using a plane-wave basis set. *Comput Mater Sci* 6:15–50.
19. Graciani J, Alvarez LJ, Rodriguez JA, Sanz JF (2008) N doping of rutile $TiO_2(110)$ surface: A theoretical DFT study. *J Phys Chem C* 112:2624–2631.
20. Fabris S, de Gironcoli S, Baroni S, Vicario G, Balducci G (2005) Taming multiple valency with density functionals: A case study of defective ceria. *Phys Rev B* 71:041101.
21. Liu G, Rodriguez JA, Hrbek J, Dvorak J, Peden CHF (2001) Electronic and chemical properties of $Ce_{0.8}Zr_{0.2}O_2(111)$ surfaces: Photoemission, XANES, density-functional, and NO_2 adsorption studies. *J Phys Chem B* 105(32):7762–7770.
22. Pfau A, Schierbaum KD (1994) The electronic-structure of stoichiometric and reduced CeO_2 surfaces—An XPS, UPS and HREELS study. *Surf Sci* 321:71–80.
23. Wang X, et al. (2008) Ceria-based catalysts for the production of H_2 through the water–gas-shift reaction: Time-resolved XRD and XAFS studies. *Top Catal* 49:81–88.
24. Jacobs G, et al. (2004) Water–gas shift: Comparative screening of metal promoters for metal/ceria systems and role of the metal. *Appl Catal A* 258:203–214.
25. Nakamura J, Campbell JM, Campbell CT (1990) Kinetics and mechanism of the water–gas shift reaction catalyzed by the clean and Cs-promoted Cu(110) surface—A comparison with Cu(111). *J Chem Soc Faraday Trans* 86:2725–2734.
26. Gokhale AA, Dumesic JA, Mavrikakis M (2008) On the mechanism of low-temperature water gas shift reaction on copper. *J Am Chem Soc* 130:1402–1414.
27. Liu P, Rodriguez JA (2007) Water–gas-shift reaction on metal nanoparticles and surfaces. *J Chem Phys* 126:164705.
28. Ojifinni RA, et al. (2008) Water-enhanced low-temperature CO oxidation and isotope effects on atomic oxygen-covered Au(111). *J Am Chem Soc* 130:6801–6812.
29. Bamwenda GR, Tsubota S, Nakamura T, Haruta M (1997) The influence of the preparation methods on the catalytic activity of platinum and gold supported on TiO_2 for CO oxidation. *Catal Lett* 44:83–87.
30. Chen MS, Goodman DW (2004) The structure of catalytically active gold on titania. *Science* 306:252–255.
31. Hernandez NC, Sanz JF, Rodriguez JA (2006) Unravelling the origin of the high-catalytic activity of supported Au: A density-functional theory-based interpretation. *J Am Chem Soc* 128:15600–15601.
32. Molina LM, Hammer B (2003) Active role of oxide support during CO oxidation at Au/MgO. *Phys Rev Lett* 90:206102.
33. Remediakis IN, Lopez N, Norskov JK (2005) CO oxidation on rutile-supported Au nanoparticles. *Angew Chem Int Ed* 44:1824–1826.